

Article

Direct Torque Control for Series-Winding PMSM with Zero-Sequence Current Suppression Capability

Zhicong Su ¹, Yuefei Zuo ² and Xiaogang Lin ^{3,*}

¹ College of Physics and Information Engineering, Quanzhou Normal University, Quanzhou 362000, China; suzhicong@qztc.edu.cn

² Department of Aeronautical and Automotive Engineering, Loughborough University, Loughborough LE11 3TU, UK; y.zuo@lboro.ac.uk

³ Quanzhou Center of Equipment Manufacturing, Haixi Institute, Chinese Academy of Sciences, Jinjiang 362216, China

* Correspondence: xiaogang_lin@fjirms.ac.cn

Abstract: The series-winding permanent-magnet synchronous motor (SW-PMSM) has the merits of high output power and excellent control performance, as does the open-winding permanent-magnet synchronous motor (OW-PMSM). Meanwhile, it can greatly reduce the number of power devices. However, due to the existence of the zero-sequence path, zero-sequence current occurs, which can cause additional losses and torque ripples. Thus, this paper proposes a novel direct torque-control strategy for the SW-PMSM with zero-sequence current suppression capability (ZSCS-DTC). First, the series-winding topology (SWT) and the voltage vector distribution in the SW-PMSM drives are analyzed. Secondly, the basic DTC (B-DTC) scheme for the SW-PMSM is investigated, and the defects of zero-sequence current open-loop control in the B-DTC scheme are revealed. Thirdly, a new voltage vector synthesis scheme is proposed for suppression of zero-sequence current while ensuring bus voltage utilization. A switching table is reconstructed with the newly synthesized voltage vectors. On this basis, a ZSCS-DTC scheme for the SW-PMSM is proposed based on zero-sequence current closed-loop control so that electromagnetic torque, stator flux linkage and zero-sequence current can be controlled simultaneously. Finally, the effectiveness of the proposed ZSCS-DTC scheme for the SW-PMSM drives is verified.

Keywords: zero-sequence current suppression; direct torque control (DTC); series-winding topology; permanent-magnet synchronous motor (PMSM)



Citation: Su, Z.; Zuo, Y.; Lin, X. Direct Torque Control for Series-Winding PMSM with Zero-Sequence Current Suppression Capability. *Electronics* **2023**, *12*, 4692. <https://doi.org/10.3390/electronics12224692>

Academic Editor: Kan Akatsu

Received: 21 October 2023

Revised: 10 November 2023

Accepted: 14 November 2023

Published: 18 November 2023



Copyright: © 2023 by the authors. Licensee MDPI, Basel, Switzerland. This article is an open access article distributed under the terms and conditions of the Creative Commons Attribution (CC BY) license (<https://creativecommons.org/licenses/by/4.0/>).

1. Introduction

Due to the merits of high efficiency, high power density, high torque output and high reliability, permanent-magnet synchronous motors (PMSMs) are widely used in transportation, industrial production and wind power generation [1–4]. However, limited by the DC-bus voltage of the driver, the operating range of traditional PMSMs is difficult to further extend with the same torque capability. The open-winding topology (OWT) was proposed to drive the motors for higher bus voltage utilization [5–7]. Such OWT-driven PMSMs are supplied by two inverters simultaneously and are associated with the advantages of multilevel voltage output and high bus voltage utilization [8–10]. However, such a drive system has twice as many power devices as the conventional drive system, resulting in considerably increased cost and volume, making it unacceptable for some applications.

In order to overcome the abovementioned defects, the SWT was proposed [11–15]. The SWT is a special open-winding structure, which multiplexes the adjacent inverter legs located in the middle of the OWT [11]. The SWT retains the advantages of high bus voltage utilization and zero-sequence controllability while greatly reducing the number of power devices so that the cost and volume can be greatly decreased, which is the main concern in industrial applications [13,16,17].

However, as the impedance of the zero-sequence loop in the SWT is very small, a small zero-sequence voltage disturbance results in undesired zero-sequence current and additional torque ripple [18]. What is more important is that the sources of zero-sequence disturbance voltage are complicated. From the inverter side, the nonlinearity of the inverter and the equivalent zero-sequence modulation voltage [10] induce zero-sequence voltage. From the machine side, zero-sequence back electromotive force (EMF) and cross-coupling voltages in zero sequence [10] also lead to zero-sequence voltage. Thus, it is difficult to completely suppress zero-sequence voltage by means of compensation. In order to avoid generating undesired zero-sequence current, voltage vectors without zero-sequence components are employed for modulation [19]. However, the zero-sequence disturbance voltages induced by the zero-sequence back EMF and the inverter nonlinearities cannot be avoided. From another perspective, the SWT has good zero-sequence controllability because the zero-sequence voltage in any direction can be injected into the zero-sequence loop in the SWT [17]. A space-vector modulation (SVM) strategy [11,20,21] is proposed for the decoupled control of the torque output and the zero-sequence current. In order to keep the modulation in zero-sequence subspace from being affected by the modulation in the α - β subspace, two virtual voltage vectors only containing zero-sequence components are synthesized by the three adjacent voltage vectors, which have the same positive or negative zero-sequence component. Therefore, the modulations in different subspaces are decoupled. However, the DC-link voltage utilization is reduced due to the separate modulations in different subspaces. In order to fully extract the output capability of the SWT, a three-dimensional space-vector modulation (3D-SVM) scheme [17] is investigated. Six specific planes are set to divide the entire feasible region of the 3D space into twenty-four subtetrahedrons [17]. By looking up the table of the relative positional relationship between the reference voltage vector and six specific planes, three adjacent basic voltage vectors can be selected to synthesize the reference voltage vector in the 3D space. However, subtetrahedron determination is intuitive but complex. In short, it can be seen that the corresponding modulation scheme is important for the control of the torque output and zero-sequence current suppression of the SW-PMSM drive.

Furthermore, the control of the SW-PMSM is quite different from that of the conventional PMSM but similar to that of the OW-PMSM [21] because they all need to suppress the zero-sequence current while controlling the torque output and the stator flux linkage. Model predictive control [21,22] and field-oriented control [23] have been promoted in SW-PMSM drives. However, in some applications, such as in electric vehicles, electric ships and robotic actuators [22], a fast dynamic response and robustness of the drive system are required, and direct torque control (DTC) can be a better candidate for SW-PMSM drives.

In [19], the B-DTC of the SW-PMSM drive was investigated. The switching table for the hysteresis controllers was rederived with six voltage vectors without zero-sequence components. However, the performance of the B-DTC scheme is affected by the zero-sequence current if the zero-sequence disturbance voltage induced by the nonlinearity of the inverter, zero-sequence back electromotive force (EMF) and cross-coupling voltages in zero sequence [10] are not completely compensated for. It is essentially an open-loop control of zero-sequence current suppression. Good performance can be obtained if those zero-sequence disturbance voltages are completely compensated for, but this is a difficult task. Therefore, it is necessary to introduce a closed-loop control system of zero-sequence current with the proper controller for active zero-sequence current suppression.

In this paper, a novel direct torque-control strategy with zero-sequence current suppression capability (ZSCS-DTC) is proposed for SW-PMSM drives. The main contributions of this work can be summarized as follows. First, the SWT and its voltage vector distribution are investigated, and the influence of voltage vectors on zero-sequence current is analyzed. Secondly, the defects and the core cause of the inevitable zero-sequence current in the B-DTC scheme for the SW-PMSM are revealed. Based on the aforementioned points, a new voltage vector synthesis scheme is proposed in this paper, and a switching table is reconstructed with the newly synthesized voltage vectors. Finally, a closed-loop control

scheme for zero-sequence current suppression is constructed so that multiobjective control electromagnetic torque, stator flux linkage and zero-sequence current can be realized in the SW-PMSM drives.

This paper is organized as follows. In Section 2, the mathematical model and voltage vector distribution of the SW-PMSM drive are introduced. In Section 3, the B-DTC scheme of the SW-PMSM drive is investigated, and the defects and the core cause of the inevitable zero-sequence current in the B-DTC scheme are revealed. In Section 4, a new voltage vector synthesis scheme is proposed, and an improved switching table is reconstructed with the newly synthesized voltage vectors. Then, the ZSCS-DTC scheme for the SW-PMSM drives is proposed based on zero-sequence current closed-loop control. In Section 5, the experimental validation is presented.

2. Mathematical Model for SW-PMSM Drives

2.1. Series-Winding PMSM Topology

The topology of the three-phase SW-PMSM drive is presented in Figure 1. The three-phase stator windings are connected in series, and the four connection points are connected to the midpoint of the four legs. The current direction is defined as positive if the current flows as shown in Figure 1.

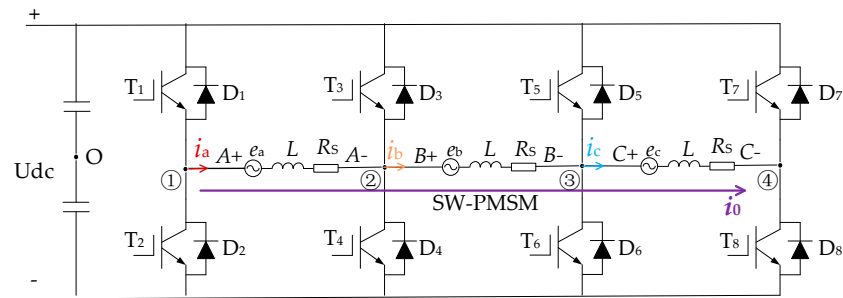


Figure 1. Series-winding topology for a three-phase SW-PMSM.

2.2. Equations of the SW-PMSM Model Considering Zero Sequence

Taking the midpoint of the DC bus as the reference ground, the stator voltage equations of the SW-PMSM can be expressed in the a-b-c stationary coordinate system as:

$$\begin{cases} u_a = e_a + L \frac{di_a}{dt} - i_a R_s = S_1 U_{dc} - S_2 U_{dc} \\ u_b = e_c + L \frac{di_b}{dt} - i_b R_s = S_2 U_{dc} - S_3 U_{dc} \\ u_c = e_c + L \frac{di_c}{dt} - i_c R_s = S_3 U_{dc} - S_4 U_{dc} \end{cases} \quad (1)$$

where e , u , I , R_s and L denote back electromotive force (EMF), voltage, current, stator resistance and inductance, respectively. Subscripts a, b and c indicate the three-phase stator winding of the SW-PMSM, respectively. S_x ($x = 1, 2, 3, 4$) indicates the switching state of the four inverter legs; when $S_x = 0$, the upper switch is turned off and the lower switch is turned on, whereas when $S_x = 1$, the upper switch is turned on and the lower switch is turned off. U_{dc} is the DC-link voltage.

If the rotor flux linkage is aligned with the direction of the phase-A winding, the stator voltage equations can be described in the d-q-0 coordinate system as follows:

$$\begin{cases} u_{sd} = R_s i_{sd} + L_d \frac{di_{sd}}{dt} - \omega_r L_q i_{sq} \\ u_{sq} = R_s i_{sq} + L_q \frac{di_{sq}}{dt} + \omega_r L_d i_{sd} + \omega_r \psi_f \\ u_{s0} = e_0 - R_s i_{s0} + L_0 \frac{di_{s0}}{dt} \end{cases} \quad (2)$$

where ω_r is the synchronous electrical angular velocity; subscripts d, q and 0 indicate the corresponding axis of the d-q-0 coordinate system, respectively; and e_0 denotes the zero-sequence component of the back EMF.

Based on Equation (2), the zero-sequence voltage in the SWT-driven PMSMs consists of the zero-sequence excitation voltage (u_{s0}) generated by the four-leg inverter and the zero-sequence back EMF (e_0) generated by the third harmonic flux density distribution. Moreover, the magnitude of the zero-sequence current is dependent on the zero-sequence voltage source and the impedance of the zero-sequence circuit.

The zero-sequence excitation voltage (u_{s0}) and the zero-sequence current (i_{s0}) can be calculated as:

$$\begin{aligned} u_{s0} &= (u_a + u_b + u_c)/3 \\ i_{s0} &= (i_a + i_b + i_c)/3 \end{aligned} \tag{3}$$

Based on Equations (1) and (3), u_{s0} can be obtained as shown in (4).

$$\begin{aligned} u_{s0} &= (S_1 - S_2 + S_2 - S_3 + S_3 - S_4) u_{dc} \\ &= (S_1 - S_4) u_{dc}/3 \end{aligned} \tag{4}$$

Based on Equation (4), when the switching states (S_1 and S_4) are not the same in one PWM cycle, the four-leg inverter outputs a zero-sequence excitation voltage (u_{s0}) on the three-phase stator winding. In addition, the magnitude of the zero-sequence excitation voltage (u_{s0}) is independent of the switching state of the second and third inverter legs. For example, when the switching state (S_2) changes, the electrical potential of the A− point and B+ point shown in Figure 1 change simultaneously, and their magnitudes remain equal and cancel each other out in Equation (4). Therefore, according to Equation (2), zero-sequence current is generated in the stator windings once the zero-sequence excitation voltage (u_{s0}) cannot cancel out the effects of the zero-sequence back EMF (e_0).

Considering the existence of zero-sequence current, the output torque (T_e) can be expressed as:

$$T_e = 1.5n_p \left[(L_d i_{sd} + \psi_f) i_{sq} + L_q i_{sq} \right] - 9n_p \psi_{3f} \sin(3\theta_r) i_{s0} \tag{5}$$

where, L_d , L_q and L_0 are the corresponding inductance in the d-q-0 coordinate system, respectively; ψ_f is the rotor flux linkage; ψ_{3f} is the amplitude of the third harmonic rotor flux linkage; and n_p is the number of pole pairs.

Based on Equation (5), the third harmonic rotor flux linkage (ψ_{3f}) and the zero-sequence current (i_{s0}) lead to torque ripple. The third harmonic rotor flux linkage is an inherent parameter of the motor. As the impedance of the zero-sequence loop in the SWT is very small, zero-sequence disturbance voltage results in zero-sequence current and torque ripple, which reduce the efficiency and stability of the SW-PMSM drive system. Therefore, it is necessary to take measures to suppress zero-sequence current for good driving performance.

2.3. Voltage Vector Distribution of SW-PMSM Drive

Unlike the conventional PMSM driven by a three-phase inverter, the SW-PMSM is driven by an inverter with four legs so that there is a total of 16 switching states. The stator phase voltages (u_A , u_B and u_C) can be expressed with the switching states as:

$$\begin{bmatrix} u_a \\ u_b \\ u_c \end{bmatrix} = U_{dc} \begin{bmatrix} S_1 - S_2 \\ S_2 - S_3 \\ S_3 - S_4 \end{bmatrix} = U_{dc} \begin{bmatrix} 1 & -1 & 0 & 0 \\ 0 & 1 & -1 & 0 \\ 0 & 0 & 1 & -1 \end{bmatrix} \begin{bmatrix} S_1 \\ S_2 \\ S_3 \\ S_4 \end{bmatrix} \tag{6}$$

According to the Clark transformation, Equation (6) can be described in the α - β -0 coordinate system as:

$$\begin{bmatrix} u_\alpha \\ u_\beta \\ u_0 \end{bmatrix} = \frac{2}{3} \begin{bmatrix} 1 & -\frac{1}{2} & -\frac{1}{2} \\ 0 & \frac{\sqrt{3}}{2} & -\frac{\sqrt{3}}{2} \\ \frac{\sqrt{2}}{2} & \frac{\sqrt{2}}{2} & \frac{\sqrt{2}}{2} \end{bmatrix} \begin{bmatrix} u_a \\ u_b \\ u_c \end{bmatrix} \tag{7}$$

Based on Equations (6) and (7), if the four inverter legs have different switching states, u_α , u_β and u_0 have different values, as presented in Table 1 [11].

Table 1. Components of voltage vectors in the $\alpha\beta 0$ subspace.

Voltage Vectors	$S_1S_2S_3S_4$	u_α/U_{dc}	u_β/U_{dc}	u_0/U_{dc}
V_0	0000	0	0	0
V_1	0001	1/3	$1/\sqrt{3}$	-1/3
V_2	0010	0	$-2/\sqrt{3}$	0
V_3	0011	1/3	$-1/\sqrt{3}$	-1/3
V_4	0100	-1	$1/\sqrt{3}$	0
V_5	0101	-2/3	$2/\sqrt{3}$	-1/3
V_6	0110	-1	$-1/\sqrt{3}$	0
V_7	0111	-2/3	0	-1/3
V_8	1000	2/3	0	1/3
V_9	1001	1	$1/\sqrt{3}$	0
V_{10}	1010	2/3	$-2/\sqrt{3}$	1/3
V_{11}	1011	1	$-1/\sqrt{3}$	0
V_{12}	1100	-1/3	$1/\sqrt{3}$	1/3
V_{13}	1101	0	$2/\sqrt{3}$	0
V_{14}	1110	-1/3	$-1/\sqrt{3}$	1/3
V_{15}	1111	0	0	0

The subscripts of the 16 voltage vectors represent the inverter switching state ($S_1S_2S_3S_4$). For example, the subscript of voltage vector V_{10} is the decimal expression of binary numbers 1010, which correspond to the switching state ($S_1S_2S_3S_4$).

Based on the amplitude of voltage vectors, the 16 voltage vectors can be classified into the following four categories. (1) Two zero-voltage vectors (V_0 and V_{15}), whose amplitude and zero-axis component are null; (2) six active voltage vectors ($V_2, V_4, V_6, V_9, V_{11}$ and V_{13}), whose amplitude is $2u_{dc}/\sqrt{3}$ and zero-axis component is null; (3) six active voltage vectors ($V_1, V_3, V_7, V_8, V_{12}$ and V_{14}), whose amplitude is $\sqrt{5}u_{dc}/3$ and zero-axis component is $\pm u_{dc}/3$; and (4) two long active voltage vectors (V_5 and V_{10}), whose amplitude is $\sqrt{17}u_{dc}/3$ and zero-axis component is $\pm u_{dc}/3$. The distribution of the 16 voltage vectors in different subspaces is shown in Figure 2.

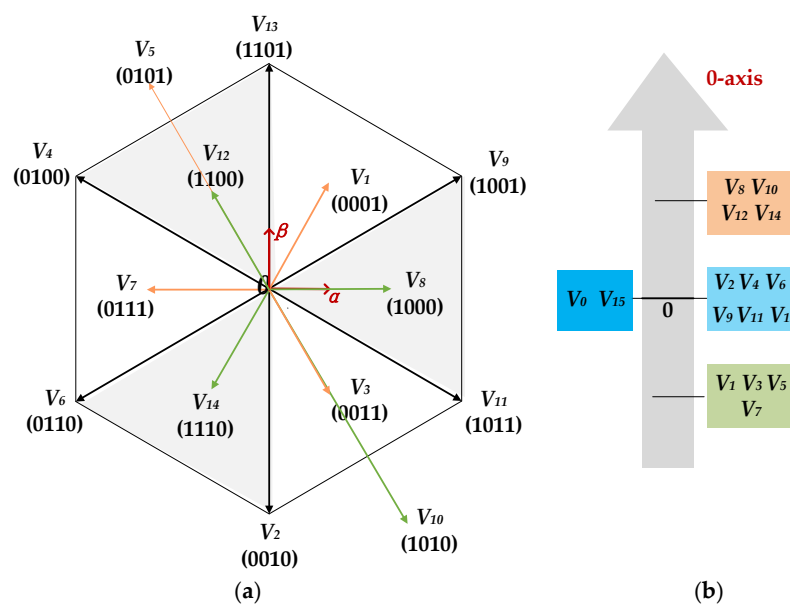


Figure 2. Voltage vector distribution of the SW-PMSM drive in the (a) $\alpha\beta$ subspace and (b) zero-sequence subspace.

Table 2. Switching table of the B-DTC.

φ	τ	Sector					
		I	II	III	IV	V	VI
$\varphi = 1$	$\tau = 1$	V_{13}	V_4	V_6	V_2	V_{11}	V_9
	$\tau = 0$	V_{11}	V_9	V_{13}	V_4	V_6	V_2
$\varphi = 0$	$\tau = 1$	V_4	V_6	V_2	V_{11}	V_9	V_{13}
	$\tau = 0$	V_2	V_{11}	V_9	V_{13}	V_4	V_6

3.2. Limitations of the B-DTC Scheme for SW-PMSM

Since the impedance of the zero-sequence circuit in the SW-PMSM drives is very small, a small zero-sequence disturbance induces a large zero-sequence current. If the zero-sequence excitation voltage (u_{s0}) cannot eliminate the negative effects of the zero-sequence back EMF (e_0) completely, zero-sequence current is induced in the zero-sequence loop. In the B-DTC scheme, the active voltage vectors with null zero-sequence components were selected to rederive the switching table in order to avoid generating zero-sequence disturbance voltage from the inverter side. However, its effect is limited because of the existence of inverter nonlinearities, such as deadtime effects.

The positive current direction of the inverter leg is defined as flowing from the inverter leg to the stator winding. During the dead time, the output voltage of each inverter leg is determined by the current polarity of the inverter leg. The output voltage of the inverter leg is 0 if the current direction is positive. The output voltage is U_{dc} if the current direction is negative. Thus, when the first and fourth inverter legs have the current directions shown in Figure 4, the deadtime effect generates a zero-sequence disturbance voltage with an amplitude of $-2U_{dc}$ on the three-phase series winding. According to the average value equivalence principle, this zero-sequence voltage is equivalent to superimposing a voltage with an average value of $-2U_{dc}T_d/T_s$ on the ideal output voltage waveform during the PWM cycle.

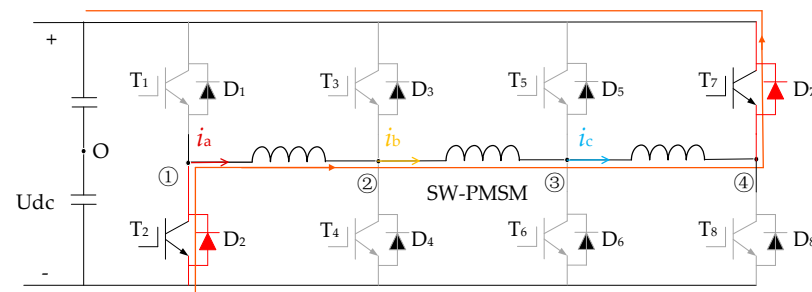


Figure 4. Zero-sequence voltage generated by the deadtime effect when $i_A > 0, i_C > 0$.

When the current directions of the first and fourth inverter legs are in other states, the zero-sequence voltages generated by the deadtime effects can be also derived as shown in Table 3.

Table 3. Zero-sequence voltage generated by the deadtime effect.

Current Direction of Phase A and C	Zero-Sequence Voltage
$i_a > 0, i_c > 0$	$-2U_{dc}T_d/T_s$
$i_a > 0, i_c < 0$	0
$i_a < 0, i_c > 0$	0
$i_a < 0, i_c < 0$	$2U_{dc}T_d/T_s$

The influence of the voltage of the deadtime effect on the three-phase series winding is shown in Figure 5, assuming that the current waveform of the three-phase winding is an ideal sine wave.

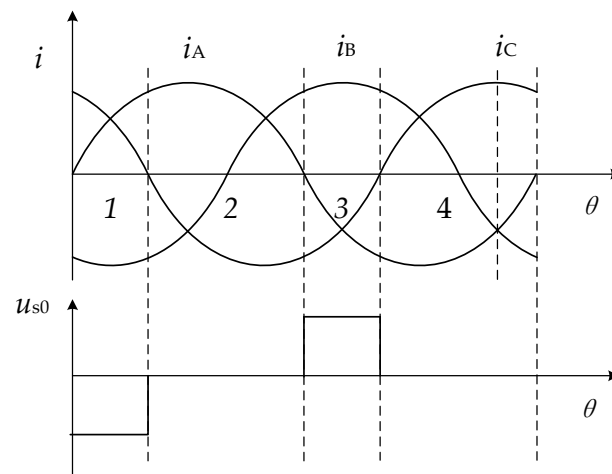


Figure 5. Zero-sequence voltage waveform generated by the deadtime effect.

At interval 1 ($i_A > 0$, $i_C > 0$; Figure 5) according to Table 3, the deadtime effects reduce the voltage of the three-phase series winding by $-2U_{dc}T_d/T_s$. At interval 3 ($i_A < 0$, $i_C < 0$), the effect of the dead time reduces the voltage of the three-phase series winding by $2U_{dc}T_d/T_s$. At the other intervals, the deadtime effect has no impact on the zero-sequence voltage.

In addition to the deadtime effects, the nonlinearity introduced by the on/off delay and the voltage drop across the power device [16,24] also causes zero-sequence disturbance voltage. The zero-sequence disturbance voltage is also associated with other factors, such as the zero-sequence back EMF and cross-coupling voltages in zero sequence [10]. It is also difficult to accurately model and completely compensate for zero-sequence disturbance.

Although the basic DTC scheme was verified by simulation results [19], it would not achieve good performance in practice for the following reasons,

(1) In the B-DTC scheme, closed-loop control systems are designed for the control of the torque and stator flux linkage, but an open-loop control mode is adopted for zero-sequence current suppression. All zero-sequence disturbance voltage should be compensated for if the zero-sequence current is to be suppressed well in open-loop control mode.

(2) There are several zero-sequence disturbance sources in the SW-PMSM drives, such as the zero-sequence back EMF, zero-sequence cross-coupling voltages, the equivalent zero-sequence modulation voltage and inverter nonlinearities [10]. More importantly, these zero-sequence disturbance sources have the characteristics of strong coupling and a nonlinear and complex cause, making it difficult to accurately model and completely compensate for such sources.

4. Proposed ZSCS-DTC for SW-PMSM Drives

4.1. Synthesis Scheme of New Voltage Vectors

According to the analysis presented in Section 2.3, as the zero-sequence path exists in the SWT, it is necessary to modulate in both α - β subspace and zero-sequence subspace. It can be seen that six voltage vectors (V_2 , V_4 , V_6 , V_9 , V_{11} and V_{13}) with no zero-sequence components are very suitable for modulation in the α - β subspace [20]. Thanks to their large amplitude of $2u_{dc}/\sqrt{3}$, the DC-bus voltage utilization is higher than that of traditional PMSM drives. However, there are no voltage vectors with null $\alpha\beta$ components in Table 1, making it difficult to independently modulate in zero-sequence subspace.

Alternatively, the concept of the virtual voltage vector [11,20] can be introduced to synthesize new voltage vectors containing only zero-sequence components. By combining V_8 , V_{12} and V_{14} and ensuring that they have the same duration during one sampling period, a virtual voltage vector with only positive zero-sequence component can be obtained [21], denoted as V_p here. The amplitude of V_p is $u_{dc}/3$. In the same way, a new virtual voltage vector with only negative zero-sequence component can be synthesized by voltage vectors

V_1, V_3 and V_7 , denoted as V_N . The amplitude of V_N is $u_{dc}/3$. Thus, virtual voltage vectors V_P and V_N have null $\alpha\beta$ component, and their zero-sequence components are in opposite directions, with an amplitude of $\pm u_{dc}/3$. More importantly, the zero-sequence subspace has only one dimension, and any required zero-sequence voltages can be modulated by these two virtual voltage vectors.

Subsequently, new synthetic voltage vectors can be obtained with a combination of two voltage vectors, one of which is selected from the six active voltage vectors ($V_2, V_4, V_6, V_9, V_{11}$ and V_{13}) with null zero-sequence components; the other is selected from virtual voltage vectors with only zero-sequence components (V_P and V_N), as shown in Figure 6.

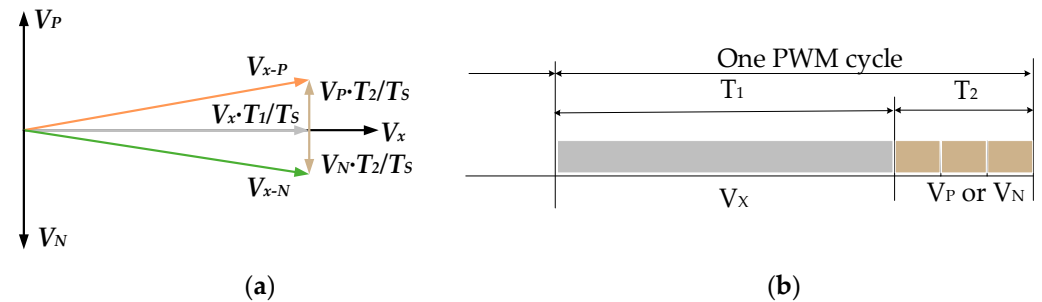


Figure 6. Synthesis of new voltage vectors: (a) synthetic voltage vectors; (b) the time allocation of the PWM cycle.

Where V_x is the voltage vector selected from the six active voltage vectors ($V_2, V_4, V_6, V_9, V_{11}$ and V_{13}); subscript x is the number of the corresponding voltage vectors; and T_1 is the duration of the selected voltage vector (V_x) in one sampling period, and its proportion in one sampling period is λ . T_2 is the duration of the virtual voltage vectors (V_P or V_N) in one sampling period, and its proportion in one sampling period is $1 - \lambda$. λ is set to 0.8 in this article, which can be changed according to practical needs. V_{x-P} and V_{x-N} are the new synthetic voltage vectors. For example, if voltage vectors V_9 and V_P are selected, their durations in one sampling time are T_1 and T_2 , respectively. Therefore, a new synthetic voltage vector can be obtained, which is denoted as V_{9-P} .

Therefore, distribution of new voltage vectors was reconstructed with these synthetic voltage vectors, as shown in Figure 7.

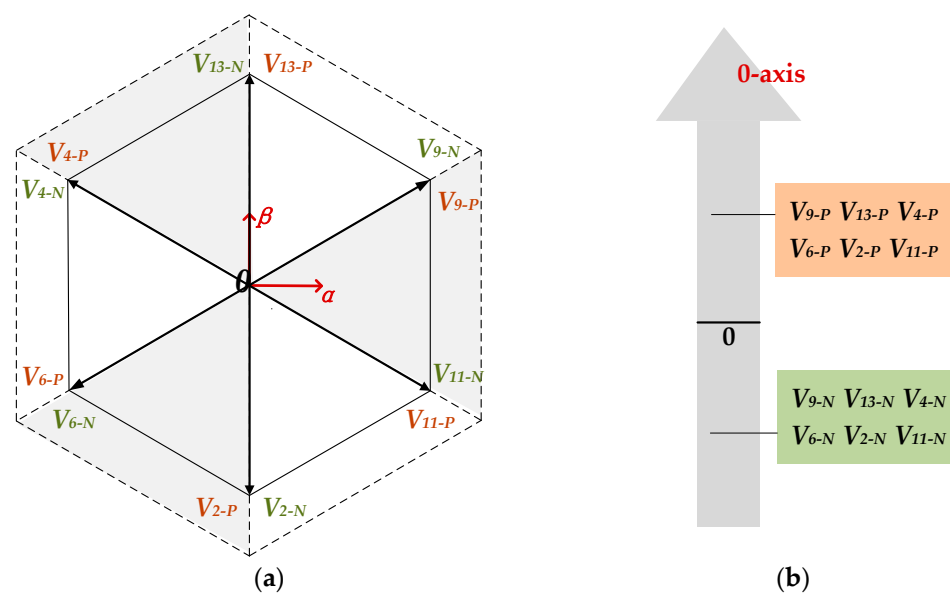


Figure 7. Voltage vector distribution with new synthesized voltage vectors in different subspaces: (a) α - β subspace; (b) zero-sequence subspace.

4.2. Closed-Loop Control of Zero-Sequence Current Suppression

In order to suppress zero-sequence current effectively, a closed-loop control scheme for zero-sequence current suppression is introduced into the DTC scheme. On this basis, a novel DTC strategy for SW-PMSM with zero-sequence current suppression capability is proposed in this section. The general control diagram of the ZSCS-DTC scheme is depicted in Figure 8.

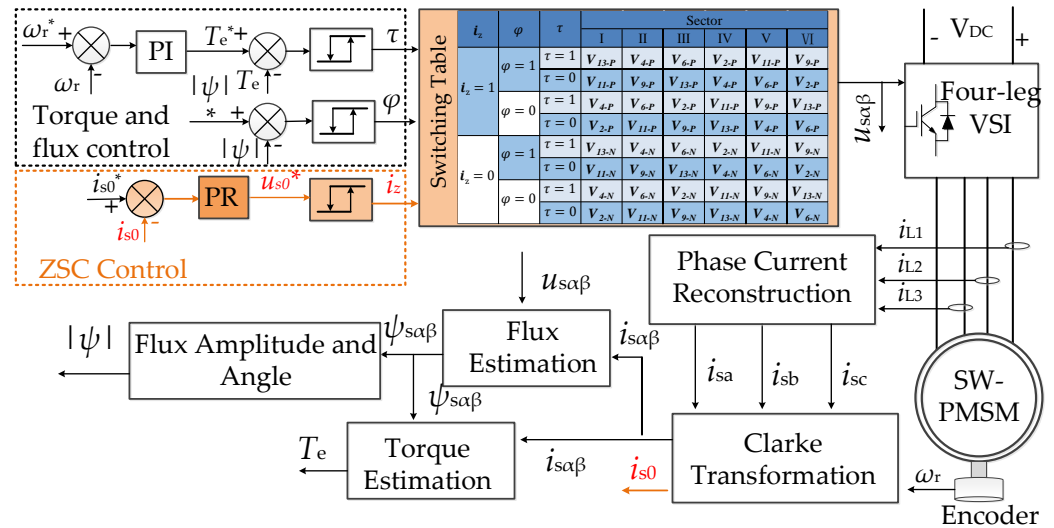


Figure 8. Proposed ZSCS-DTC architecture for the SW-PMSM drive.

Although the control process of the torque and stator flux linkage is similar to the B-DTC scheme for conventional PMSM, the proposed ZSCS-DTC strategy is fundamentally different from the B-DTC. There are two main differences:

- (1) A new voltage vector synthesis scheme is proposed for suppression of the zero-sequence current while ensuring bus voltage utilization. The switching table is reconstructed with the newly synthesized voltage vectors.
- (2) Closed-loop control of zero-sequence current suppression is introduced in the ZSCS-DTC scheme for SW-PMSM so that the zero-sequence current can be suppressed actively and the torque and stator flux linkage can be effectively controlled.

A closed-loop control scheme for zero-sequence current suppression was designed using a proportional and resonant (PR) regulator [25] and a hysteresis controller, as shown in Figure 8. Since the zero-sequence disturbance induced by the rotor harmonic flux is mainly a triple-frequency AC component [25,26], a proportional and resonant (PR) regulator is used to determine the required value of zero-sequence excitation voltage (u_{s0}) from the four-leg inverter side based on the difference between the zero-sequence current (i_{s0}) and the reference zero-sequence current (i_{s0}^*). Subsequently, the zero-sequence current control signal (i_z) can be obtained through the hysteresis controller of the zero-sequence current.

If $i_z = 1$, then the actual zero-sequence current is smaller than the reference value, the required value of u_{s0} is positive and synthetic voltage vectors (V_{x-p}) that contain positive zero-sequence components are selected to suppress the zero-sequence current, such as synthetic voltage vector V_{9-p} for. Voltage vector V_{9-p} is synthesized by voltage vectors V_9 and V_P , and voltage vector V_P is synthesized by active voltage vectors V_8 , V_{12} and V_{14} with the same duration in one PWM cycle. Thus, according to the principle of volt-second balance, the zero-sequence voltage output from the four-leg inverter in one sampling time can be calculated as

$$V_{9-p,0} \cdot T_S = T_1 \cdot V_{9,0} + T_2 \cdot V_{P,0} = T_2 \cdot V_P \tag{10}$$

where $V_{9-p,0}$, $V_{9,0}$ and $V_{P,0}$ are the zero-sequence components of the corresponding voltage vectors (V_{9-p} , V_9 and V_P).

This zero-sequence voltage ($V_{9-P,0}$) leads to positive zero-sequence current, as shown in Figure 9a. Thus, the existing negative zero-sequence current is eliminated.

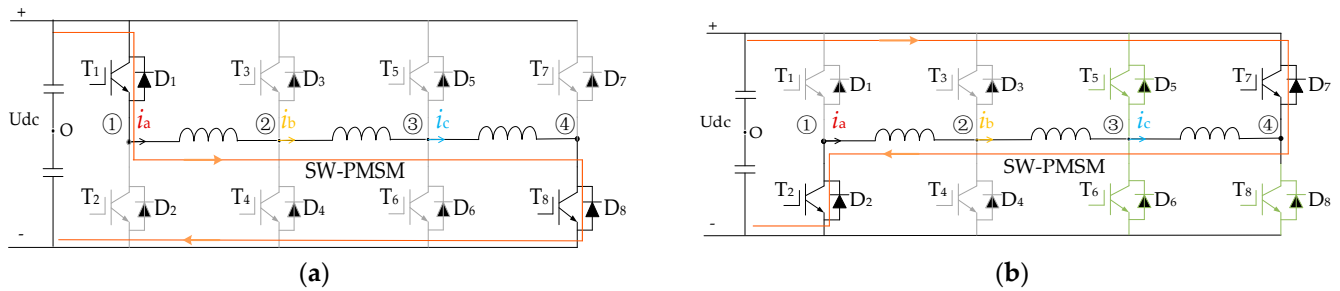


Figure 9. Zero-sequence current flow path with (a) V_{x-P} and (b) V_{x-N} .

In the same way, if $i_z = 0$, then the actual zero-sequence current is greater than the reference value, the required value of u_{s0} is negative and synthetic voltage vectors (V_{x-N}) that contain positive zero-sequence components are selected to suppress zero-sequence current, such as synthetic voltage vector V_{9-N} . Zero-sequence voltage output from the four-leg inverter in one sampling time can also be calculated as

$$V_{9-N,0} \cdot T_S = T_1 \cdot V_{9,0} + T_2 \cdot V_{N,0} = T_2 \cdot V_N \tag{11}$$

where $V_{9-N,0}$, $V_{9,0}$ and $V_{N,0}$ are the zero-sequence components of the corresponding voltage vectors (V_{9-N} , V_9 and V_N).

This zero-sequence voltage ($V_{9-N,0}$) induces negative zero-sequence current, as shown in Figure 9b. Thus, the existing positive zero-sequence current is eliminated.

Based on (10) and (11), the zero-sequence voltages generated by the synthetic voltage vectors are only associated with voltage vectors V_P and V_N .

4.3. Closed-Loop Control of the Torque and Stator Flux Linkage

Based on the analysis presented in Section 4.1, the new synthesized voltage vectors were selected as the candidates. The sector division of the α - β subspace is depicted in Figure 10. In the α - β subspace, the whole plane is divided into six identical sectors by dashed lines.

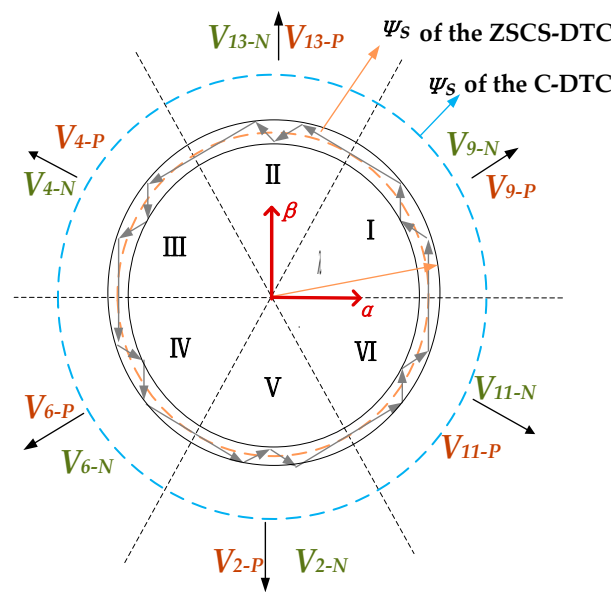


Figure 10. Sector division and the flux linkage trajectory in the α - β subspace.

Closed-loop control schemes were also designed for the torque and stator flux linkage using proportional and integral (PI) regulators and hysteresis controllers. The overall control process of the electromagnetic torque and stator flux linkage in the ZSCS-DTC scheme of the SW-PMSM drive is similar to that in the B-DTC scheme. However, the switching table should be rederived with the new synthetic voltage vectors, as shown in Table 4.

Table 4. Switching table of the ZSCS-DTC.

i_z	φ	τ	Sector					
			I	II	III	IV	V	VI
1	1	1	V_{13-P}	V_{4-P}	V_{6-P}	V_{2-P}	V_{11-P}	V_{9-P}
		0	V_{11-P}	V_{9-P}	V_{13-P}	V_{4-P}	V_{6-P}	V_{2-P}
	0	1	V_{4-P}	V_{6-P}	V_{2-P}	V_{11-P}	V_{9-P}	V_{13-P}
		0	V_{2-P}	V_{11-P}	V_{9-P}	V_{13-P}	V_{4-P}	V_{6-P}
0	1	1	V_{13-N}	V_{4-N}	V_{6-N}	V_{2-N}	V_{11-N}	V_{9-N}
		0	V_{11-N}	V_{9-N}	V_{13-N}	V_{4-N}	V_{6-N}	V_{2-N}
	0	1	V_{4-N}	V_{6-N}	V_{2-N}	V_{11-N}	V_{9-N}	V_{13-N}
		0	V_{2-N}	V_{11-N}	V_{9-N}	V_{13-N}	V_{4-N}	V_{6-N}

In Table 4, i_z is the output of the hysteresis controller for zero-sequence current. If $i_z = 0$, then the actual zero-sequence current is greater than the reference value and vice-versa.

According to the signals generated by the hysteresis controllers (i_z , φ and τ), one proper voltage vector is selected from Table 4, such as synthetic voltage vector V_{9-P} . According to the principle of volt-second balance, the $\alpha\beta$ component of the voltage output from the four-leg inverter in one sampling time can be calculated as

$$V_{9-P,\alpha\beta} \cdot T_S = T_1 \cdot V_{9,\alpha\beta} + T_2 \cdot V_{P,\alpha\beta} = T_1 \cdot V_{9,\alpha\beta} \tag{12}$$

where $V_{9-P,\alpha\beta}$, $V_{9,\alpha\beta}$ and $V_{P,\alpha\beta}$ are the $\alpha\beta$ components of the corresponding voltage vectors (V_{9-P} , V_9 and V_P).

In the same way, given the synthetic voltage vector selected from Table 4 (V_{9-N}), the $\alpha\beta$ component of the voltage output from the four-leg inverter in one sampling time can be calculated as

$$V_{9-N,\alpha\beta} \cdot T_S = T_1 \cdot V_{9,\alpha\beta} + T_2 \cdot V_{N,\alpha\beta} = T_1 \cdot V_{9,\alpha\beta} \tag{13}$$

where $V_{9-N,\alpha\beta}$ and $V_{N,\alpha\beta}$ are the $\alpha\beta$ components of the corresponding voltage vectors (V_{9-N} and V_N).

The $\alpha\beta$ component is only associated with the voltage vectors (V_x) that result in the desired electromagnetic torque and stator flux linkage. In addition, this $\alpha\beta$ component of the voltage vector does not induce zero-sequence current, so that the existing zero-sequence currents stay the same, as shown in Figure 11.

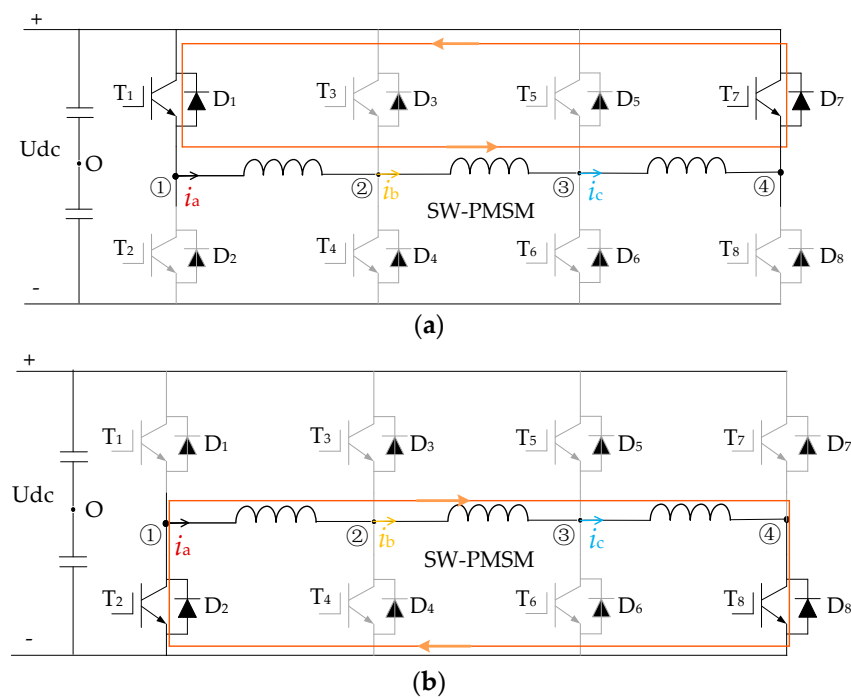


Figure 11. Zero-sequence voltage flow path during control of the torque and stator flux linkage with (a) V_P and (b) V_N .

5. Experimental Results

5.1. The Experimental Platform

In order to research the control effectiveness of the proposed ZSCS-DTC scheme for SW-PMSM drives, an experimental platform was established, as shown in Figure 12. The SW-PMSM is a conventional Y-connected PMSM in which the neutral point of the phase windings is opened and three-phase windings are connected in series. A magnetic powder brake is selected as the load. The control system is implemented in the DSP of TMS320F28335 from Texas Instrument. The sampling frequency is set to 10 kHz, and the switching frequency of the power devices is 10 kHz. The current measurement is taken with hall-effect sensors, and the waveforms of the torque, stator flux linkage and current are obtained by digital-to-analog conversion (DAC). The hysteresis comparator bands of electromagnetic torque, stator flux linkage and zero-sequence current are set to zero. The electrical parameters of the SW-PMSM are measured by an LCR meter under 1 kHz. Parameters of the PR, PI regulator of the SW-PMSM drive system are listed in Table 5.

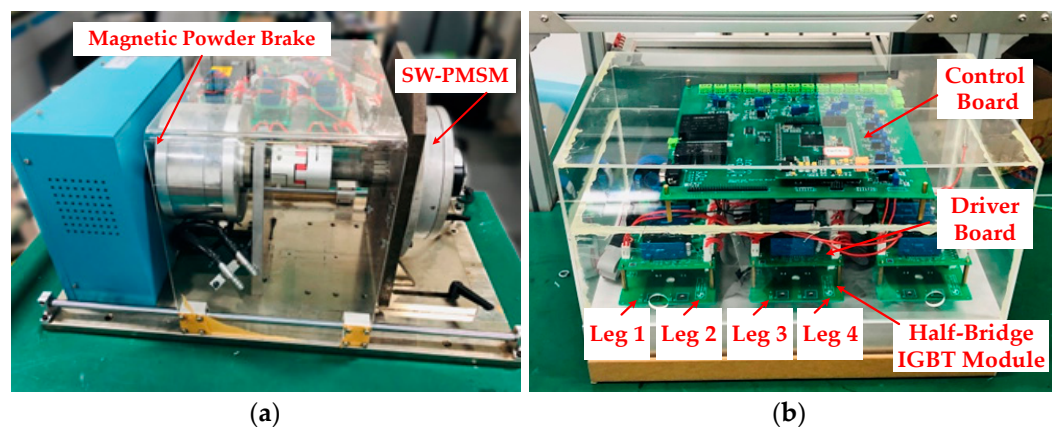


Figure 12. Experimental platform of the ZSCS-DTC for SW-PMSM drives. (a) the testbed; (b) four-leg inverter.

Table 5. Data on three-phase SW-PMSM.

Parameter	Value	Parameter	Value
Rated voltage/V	220	Phase-winding self-inductance/mH	56
Rated current/A	1.8	Proportional factor of PR regulator k_{P1}	3
Rated speed/(r/min)	300	Resonant factor of PR regulator k_R	10
Rated torque/(N·m)	10	Cutoff frequency ω_C (rad/s)	5
Stator resistance/ Ω	2.8	Proportional factor of PI regulator k_{P2}	0.4
Number of pole pairs	4	Integral factor of PI regulator k_I	1

In order to verify the control performance of the ZSCS-DTC for SW-PMSM proposed in this paper, both the B-DTC strategy and ZSCS-DTC strategy were adopted for steady-state and dynamic experiments. An experimental performance comparison is presented as follows.

5.2. Steady-State Experimental Results

Steady-state experiments were conducted to test the zero-sequence current suppression performance with the two control strategies, as shown in Figure 13. The speed of the SW-PMSM was set to 100 r/min, and the load torque was 2.5 N·m.

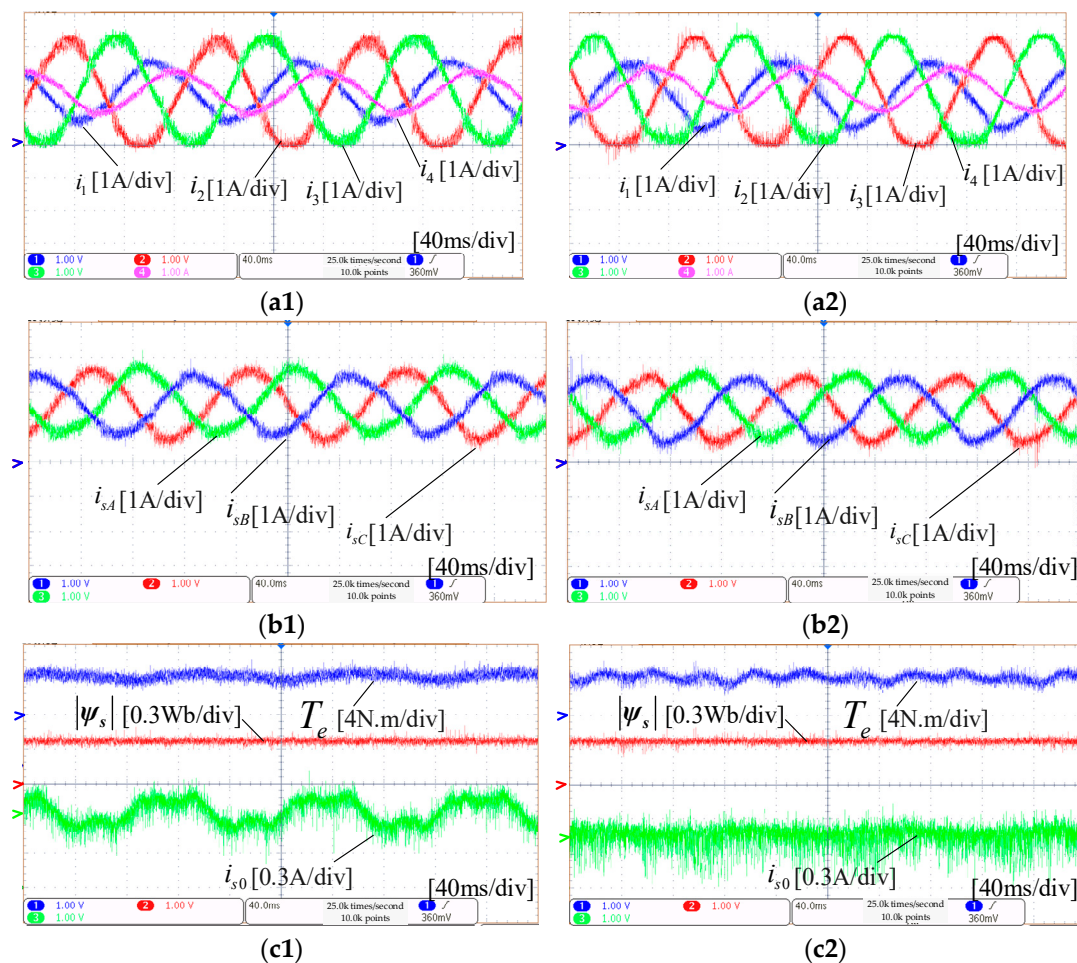


Figure 13. Steady-state response under 100 r/min with different control schemes: (a1) Inverter-leg current with the B-DTC; (a2) Inverter-leg current with the ZSCS-DTC; (b1) Three-phase stator current with the B-DTC; (b2) Three-phase stator current with the ZSCS-DTC; (c1) Torque, stator flux linkage and zero-sequence current with the B-DTC; (c2) Torque, stator flux linkage and zero-sequence current with the ZSCS-DTC.

The currents of inverter legs were measured with hall-effect sensors and sent to the DSP. The three-phase currents were reconstructed with the measured currents of inverter legs. The current waveforms were obtained by digital-to-analog conversion (DAC). Limited by the DAC output range of 0–3.3 V, a DC offset was superimposed on the currents in the DSP chip. The current waveforms of inverter legs with the B-DTC strategy and the ZSCS-DTC strategy are shown in Figure 13(a1) and Figure 13(a2), respectively. The three-phase current waveforms with the B-DTC strategy and ZSCS-DTC strategy are shown in Figure 13(b1) and Figure 13(b2), respectively. The waveforms of the torque, stator flux linkage and zero-sequence current with different strategies are shown in Figure 13(c1,c2). It can be seen that both control strategies can ensure small fluctuations of the torque and stator flux linkage. The zero-sequence current with the B-DTC strategy keeps the fluctuation within the range of 0 ± 0.25 A; moreover, the zero-sequence current with the proposed ZSCS-DTC strategy keeps the fluctuation within the range of 0 ± 0.12 A. Thus, we conclude that the proposed ZSCS-DTC strategy achieves better performance than the B-DTC strategy under steady-state operation in terms of zero-sequence current suppression, while the stator flux linkage and torque are kept in a small fluctuation range.

5.3. Dynamic Experimental Results

Load step experiments were carried out to test the control performance of zero-sequence current suppression during the transient process. Figure 14a,b are the load step experimental results with the B-DTC strategy and the proposed ZSCS-DTC strategy, respectively. The load steps abruptly from 4 N m to 0 N m at 100 r/min. It can be seen that the zero-sequence current with the B-DTC (Figure 14a) was reduced from 0.25 A to 0.15 A, while the zero-sequence current with the proposed ZSCS-DTC (Figure 14b) fluctuated within the range of 0 ± 0.125 A. Therefore, the zero-sequence current was suppressed well during the transient load step process.

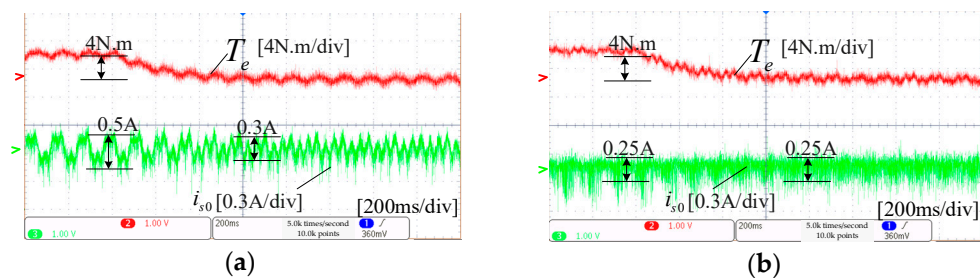


Figure 14. Dynamic response under varying torque with different control schemes: (a) B-DTC; (b) ZSCS-DTC.

Speed step experiments were also carried out, as shown in Figure 15. While the speed setpoint suddenly increased from 20 r/min to 100 r/min, the speed can rise rapidly and enter the stable state. However, the zero-sequence current amplitude with the B-DTC (Figure 15a) increased from 0.1 A to 0.25 A, while the zero-sequence current with the proposed ZSCS-DTC (Figure 15b) fluctuated within the range of 0 ± 0.125 A. Therefore, the experimental results presented in Figure 15a,b verify that the proposed ZSCS-DTC strategy can effectively suppress the zero-sequence current while maintaining fast dynamic response capability during the transient speed step process.

Overall, the comparative experimental results verify that the proposed ZSCS-DTC achieves better performance than the B-DTC in the transient process of load change or speed change in suppressing zero-sequence current. In addition, the zero-sequence current suppression is decoupled from the control of the torque and stator flux linkage.

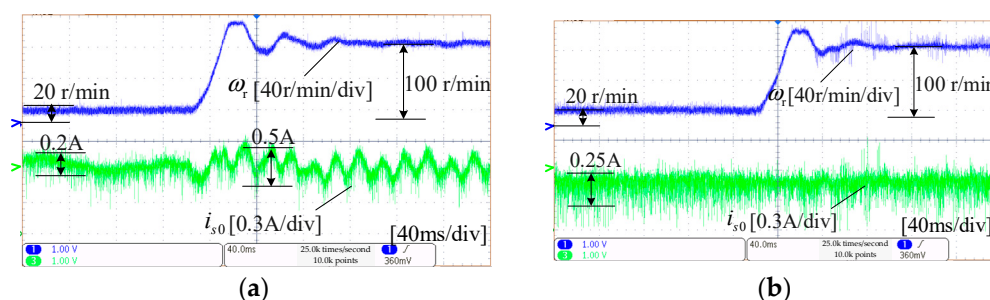


Figure 15. Dynamic response under varying speeds with different control schemes: (a) B-DTC; (b) ZSCS-DTC.

6. Conclusions

Since the zero-sequence path exists in SW-PMSM drives, zero-sequence current occurs and induces additional losses and torque ripples. Meanwhile, the B-DTC strategy cannot suppress the zero-sequence current well under an open-loop control mode of zero-sequence current because the zero-sequence disturbance is difficult to compensate for completely. With the aim of obtaining superior control performance of the electromagnetic torque, stator flux linkage and zero-sequence current suppression, the main contributions of this paper are summarized as follows.

(1) The voltage vector distribution of the SWT was analyzed, and zero-sequence voltage disturbance sources in the SW-PMSM drives were introduced in detail. The B-DTC strategy for the SW-PMSM drives was investigated, and the reason why the zero-sequence current cannot be actively suppressed actively was revealed, which is that an open-loop control mode was adopted to suppress zero-sequence current in the B-DTC scheme.

(2) A new voltage vector synthesis scheme was proposed for the simultaneous control of the electromagnetic torque, stator flux linkage and zero-sequence current suppression while ensuring the bus voltage utilization. The switching table was reconstructed with the newly synthesized voltage vectors. On this basis, the ZSCS-DTC strategy is proposed for SW-PMSM drives based on closed-loop control of the zero-sequence current so that electromagnetic torque, stator flux linkage and zero-sequence current can be controlled simultaneously.

Steady-state and dynamic experiments were carried out with the B-DTC strategy and the ZSCS-DTC strategy. The comparative experiments verify that the zero-sequence current is effectively suppressed under the premise of the torque and stator flux linkage being correctly controlled with the proposed ZSCS-DTC strategy.

Author Contributions: Conceptualization, Z.S. and X.L.; Data curation, Y.Z.; Formal analysis, Z.S. and X.L.; Funding acquisition, Z.S. and X.L.; Investigation, Z.S.; Methodology, Y.Z.; Project administration, Z.S., Y.Z. and X.L.; Software, X.L.; Supervision, X.L.; Validation, Z.S., Y.Z. and X.L.; Visualization, Z.S.; Writing—original draft, Z.S. and X.L.; Writing—review and editing, Y.Z. and X.L. All authors have read and agreed to the published version of the manuscript.

Funding: This research was funded in part by the Educational Research Program for Young and Middle-aged Teachers from Fujian Provincial Department of Education under Grant No. JAT200559, in part by the Fujian Provincial Natural Science Fund under Grant No. 2021J05105, in part by the Quanzhou Science and Technology Plan under Grant No. 2021C025R and in part by Supporting Project of the STS Program of the Chinese Academy of Sciences in Fujian Province under Grant No. 2023T3015.

Data Availability Statement: Data are contained within the article.

Conflicts of Interest: The authors declare no conflict of interest.

References

1. Liu, C.; Chau, K.T.; Lee, C.H.T.; Song, Z. A Critical Review of Advanced Electric Machines and Control Strategies for Electric Vehicles. In *Proceedings of the IEEE*; IEEE: Piscataway, NJ, USA, 2021; Volume 109, pp. 1004–1028.
2. Lemma, B.D.; Pradabane, S. An Optimized Alternative Fixed Switching 12-Sector Space Vector Pulse Width Modulation Control of Open-End Winding PMSM Drive. *IEEE Access* **2023**, *11*, 55169–55177. [[CrossRef](#)]
3. Wang, X.; Lin, X.; Huang, Q.; Xie, W. An Improved Parallel Predictive Torque Control for Permanent Magnet Synchronous Motor. *IEEE Access* **2023**, *11*, 32496–32507. [[CrossRef](#)]
4. Bao, G.; Qi, W.; He, T. Direct Torque Control of PMSM with Modified Finite Set Model Predictive Control. *Energies* **2020**, *13*, 234. [[CrossRef](#)]
5. Takahashi, I.; Ohmori, Y. High-performance direct torque control of an induction motor. *IEEE Trans. Ind. Appl.* **1989**, *25*, 257–264. [[CrossRef](#)]
6. Stemmler, H.; Guggenbach, P. Configurations of high-power voltage source inverter drives. In Proceedings of the 1993 Fifth European Conference on Power Electronics and Applications, Brighton, UK, 13–16 September 1993; Volume 5, pp. 7–14.
7. Yuan, X.; Zhang, C.; Zhang, S. Torque Ripple Suppression for Open-End Winding Permanent-Magnet Synchronous Machine Drives with Predictive Current Control. *IEEE Trans. Ind. Electron.* **2020**, *67*, 1771–1781. [[CrossRef](#)]
8. Shen, Z.; Jiang, D.; Zhu, L.; Xu, Y.; Zou, T.; Liu, Z.; Qu, R.A. Novel Zero-Sequence Current Elimination PWM Scheme for an Open-Winding PMSM with Common DC Bus. *IEEE Trans. Power Electron.* **2019**, *34*, 12476–12490. [[CrossRef](#)]
9. Hu, W.; Nian, H.; Sun, D. Zero-Sequence Current Suppression Strategy with Reduced Switching Frequency for Open-End Winding PMSM Drives with Common DC BUS. *IEEE Trans. Ind. Electron.* **2018**, *66*, 7613–7623. [[CrossRef](#)]
10. Zhan, H.; Zhu, Z.-q.; Odavic, M. Analysis and Suppression of Zero Sequence Circulating Current in Open Winding PMSM Drives with Common DC Bus. *IEEE Trans. Ind. Appl.* **2017**, *53*, 3609–3620. [[CrossRef](#)]
11. Li, A.; Jiang, D.; Kong, W.; Qu, R. Four-leg converter for reluctance machine with DC-biased sinusoidal winding current. *IEEE Trans. Power Electron.* **2019**, *34*, 4569–4580. [[CrossRef](#)]
12. Li, A.; Jiang, D.; Liu, Z.; Kong, W. Five-phase Series-end Winding Motor Controller: Converter Topology and Modulation Method. In Proceedings of the 2019 IEEE Energy Conversion Congress and Exposition (ECCE), Baltimore, MD, USA, 29 September–3 October 2019; pp. 629–634.
13. Li, A.; Jiang, D.; Liu, Z.; Sun, X.; Kong, W. Unified Analysis of Winding Connection Sequence in Series-End Winding Topology. *IEEE Trans. Ind. Appl.* **2021**, *57*, 516–527. [[CrossRef](#)]
14. Song, Z.; Liu, C.; Dong, Z.; Huang, R. Improved Multi-Stage Decoupling Space Vector Modulation for Asymmetrical Multi-Phase PMSM With Series Winding Connection. *IEEE Trans. Power Electron.* **2022**, *37*, 10951–10966. [[CrossRef](#)]
15. Qu, H.; Li, B.; Zhou, M.; Jiang, D.; Sun, W. Impedance Identification Signal Excitation for Series-End Winding Motor System. In Proceedings of the 2023 11th International Conference on Power Electronics and ECCE Asia (ICPE 2023—ECCE Asia), Jeju, Republic of Korea, 22–25 May 2023; pp. 3138–3143.
16. Guo, Q.; Dong, Z.; Liu, H.; You, X. Nonlinear Characteristics Compensation of Inverter for Low-Voltage Delta-Connected Induction Motor. *Energies* **2020**, *13*, 590. [[CrossRef](#)]
17. Dong, Z.; Liu, C. Three-Dimension Space Vector Modulation for Three-Phase Series-End Winding Voltage-Source Inverters. *IEEE Trans. Ind. Electron.* **2023**, *71*, 82–92. [[CrossRef](#)]
18. Liu, S.; Liu, Y.; Zhang, B.; Liu, C. Full-Speed Region Predictive Current Control Method of Symmetrical Series-Winding PMSM with Higher DC-Link Utilization. *IEEE Trans. Ind. Electron.* **2023**, *early access*. [[CrossRef](#)]
19. Dong, Z.; Zhao, H.; Wen, H.; Liu, C. Direct Torque Control in Series-End Winding PMSM Drives. In Proceedings of the IECON 2022—48th Annual Conference of the IEEE Industrial Electronics Society, Brussels, Belgium, 17–20 October 2022; pp. 1–6.
20. Dong, Z.; Liu, C.; Liu, S.; Song, Z. Deadbeat predictive current control for series-winding PMSM drive with half-bridge power module-based inverter. *Energies* **2021**, *14*, 4620. [[CrossRef](#)]
21. Dong, Z.; Huang, R.; Chen, Z.; Liu, C. Active Zero-Sequence Current Suppression-Based Model Predictive Current Control for Series-End Winding PMSM Drives. In Proceedings of the 2023 IEEE International Conference on Predictive Control of Electrical Drives and Power Electronics (PRECEDE), Wuhan, China, 16–19 June 2023; pp. 1–6.
22. Dong, Z.; Chen, Y.; Feng, K.; Liu, C. Multivector-Based Model Predictive Current Control with Zero-Sequence Current Suppression for Three-Phase Series-End Winding Permanent Magnet Synchronous Motor Drives. *IEEE Trans. Transp. Electrif.* **2023**, *9*, 3282–3294. [[CrossRef](#)]
23. Li, A.; Jiang, D.; Liu, Z.; Sun, X. Generalized PWM Method for Series-End Winding Motor Drive. *IEEE Trans. Power Electron.* **2021**, *36*, 4452–4462. [[CrossRef](#)]
24. Gong, L.M.; Zhu, Z.Q. Modeling and compensation of inverter nonlinearity effects in carrier signal injection-based sensorless control methods from positive sequence carrier current distortion. In Proceedings of the 2010 IEEE Energy Conversion Congress and Exposition, Atlanta, GA, USA, 12–16 September 2010; pp. 3434–3441.

25. Sun, D.; Chen, W.; Cheng, Y.; Nian, H. Improved Direct Torque Control for Open-Winding PMSM System Considering Zero-Sequence Current Suppression with Low Switching Frequency. *IEEE Trans. Power Electron.* **2021**, *36*, 4440–4451. [[CrossRef](#)]
26. Zhou, Y.; Nian, H. Zero-Sequence Current Suppression Strategy of Open-Winding PMSG System with Common DC Bus Based on Zero Vector Redistribution. *IEEE Trans. Ind. Electron.* **2015**, *62*, 3399–3408. [[CrossRef](#)]

Disclaimer/Publisher’s Note: The statements, opinions and data contained in all publications are solely those of the individual author(s) and contributor(s) and not of MDPI and/or the editor(s). MDPI and/or the editor(s) disclaim responsibility for any injury to people or property resulting from any ideas, methods, instructions or products referred to in the content.